

Persistence of polar distortion with electron doping in lone-pair driven ferroelectricsXu He¹ and Kui-juan Jin^{1,2,*}¹*Beijing National Laboratory for Condensed Matter Physics, Institute of Physics, Chinese Academy of Sciences, Beijing 100190, China*²*Collaborative Innovation Center of Quantum Matter, Beijing 100190, China*

(Received 24 March 2016; revised manuscript received 9 October 2016; published 27 December 2016)

Free electrons can screen out long-range Coulomb interaction and destroy the polar distortion in some ferroelectric materials, whereas the coexistence of polar distortion and metallicity were found in several non-central-symmetric metals (NCSMs). Therefore, the mechanisms and designing of NCSMs have attracted great interest. In this work, by first-principles calculation, we found the polar distortion in the lone-pair driven ferroelectric material PbTiO_3 cannot only persist but also increase with electron doping. We further analyzed the mechanisms of the persisting of the polar distortion. We found that the Ti site polar instability is suppressed, but the Pb site polar instability is intact with the electron doping. The Pb-site instability is due to the lone-pair mechanism which can be viewed as a pseudo-Jahn-Teller effect, a mix of the ground state and the excited state by ion displacement from the central symmetric position. The lone-pair mechanism is not strongly affected by the electron doping because neither the ground state nor the excited state involved is at the Fermi energy. The enhancement of the polar distortion is related to the increasing of the Ti ion size by doping. These results show that the long-pair stereoactive ions can be used for designing NCSMs.

DOI: [10.1103/PhysRevB.94.224107](https://doi.org/10.1103/PhysRevB.94.224107)**I. INTRODUCTION**

In ferroelectric materials, there is a delicate balance between the short-range repulsion which favors the nonpolar structure and the long-range Coulomb interaction which favors the ferroelectric state [1,2]. Free carriers screen out the long-range Coulomb interaction, thus they can reduce the polar distortion. For example, in a prototypical ferroelectric material BaTiO_3 , the ferroelectric distortion is weakened with electron doping, and eventually disappears when a critical concentration is reached [3–6]. The screening of the Coulomb interaction was believed to be the reason for the weakening or disappearing of the polar distortion for BaTiO_3 [5,6]. Although the screening effect of the carriers can also inhibit the polar distortion in many other ferroelectric materials, there are exceptions which have attracted a lot of attentions and efforts. Anderson and Blount pointed out that while free electrons can screen out the electric field, the transverse optical soft phonons can lead to polar distortion [7]. A few “ferroelectric” metals, or more precisely non-central-symmetric metals (NCSMs) have been found or proposed, such as perovskite structure LiOsO_3 [8–12], MgReO_3 [10], and the cation-ordered $\text{SrCaRu}_2\text{O}_6$ [13]. The possible mechanisms of the NCSMs have been discussed by several authors. Xiang suggested that the long-range Coulomb interaction is not necessary for the polar distortion; the short-range pair interactions, which are not screened out by free electrons, can drive the polar distortion [10]. Puggioni and Rondinelli proposed that the non-centrosymmetric structure can exist if the coupling of the soft phonon mode and the electrons at the Fermi level is weak [13]. Benedek and Birol proposed that polar distortion can emerge through a geometric mechanism in metals [14].

Although the NCSM structures are no longer suitable for the usage as ferroelectric materials because of the metallicity, other interesting properties are found in NCSMs, like the

unconventional optical responses [15,16], magnetoelectricity [17], superconductivity [18], and thermoelectricity [13]. A deeper understanding of the mechanisms of NCSM could help finding new NCSMs. The purpose of this work is to seek a possible mechanism of NCSMs so new NCSMs can be found or designed. In this work, by studying the polar distortion in electron-doped PbTiO_3 , we show that the lone-pair driven polar distortion is compatible with metallicity. The lone pair mechanism for the polar distortion in nondoped PbTiO_3 has been long studied [19–22]. In PbTiO_3 , the hybridization between the Pb ($6s$, $6p$) bands and O $2p$ bands reduces the short-range repulsion, resulting in a large polar distortion, which is often referred to as lone-pair driven ferroelectricity. The lone-pair driven ferroelectricity can be interpreted as the result of the Pseudo-Jahn-Teller effect (PJTE) [23–26] which is local. Therefore, it is possible that the lone pair mechanism can still drive the polar distortion even if the long-range interaction is screened. We found that the polar distortion in PbTiO_3 not only persists but also is enhanced with the electron doping. Then by analyzing the evolution of the phonon and the force constant matrices (FCM’s), we found that the A-site instability, which is caused by the lone-pair mechanism, is responsible for the persisting of the polar distortion, because the electronic states involved are far away from the Fermi energy. We showed that enhancement of the polar distortion is related to the increasing of the Pb-O distance. We discussed the generalizability of the results from PbTiO_3 to other lone-pair driven ferroelectric materials and propose that the lone-pair stereoactive ions can be used for the designing of NCSMs.

II. METHODS

The density functional theory (DFT) calculations were carried out by using the projected augmented wave (PAW) [27] pseudopotentials as implemented in the Vienna *ab initio* simulation package (VASP) [28]. The energy cutoff of the plane wave basis set was 500 eV. The exchange-correlation functional with local density approximation (LDA) as parameterized by Perdew and Zunger (PZ) [29] was used. The

*Correspondence and requests for materials should be addressed to Kui-juan Jin: kjjin@iphy.ac.cn

TABLE I. Born effective charge of PbTiO_3 in cubic structure. The unit is $|e|$. Only the xx , yy , and zz part of the BEC tensors are nonzero. For Pb and Ti, $Z_{xx}^* = Z_{yy}^* = Z_{zz}^*$. For O, $Z_{O1,yy}^* = Z_{O1,xx}^* = Z_{O2,yy}^* = Z_{O2,zz}^*$, $Z_{O2,xx}^* = Z_{O1,zz}^*$. The results in Ref. [37] were calculated with LDA/DFPT.

	Z_{Pb}^*	Z_{Ti}^*	$Z_{O1,xx}^*$	$Z_{O1,zz}^*$
This work	3.92	7.25	-2.62	-5.94
Ref. [37]	3.90	7.06	-2.56	-5.83

reference electronic configurations for the pseudopotentials are Pb $5d^{10}6s^26p^2$, Ba $5s^25p^66s^2$, Ti $3s^23p^63d^4$, and O $2s^22p^6$, respectively. An $8 \times 8 \times 8$ Γ -centered k -point mesh was used to represent the reciprocal space. The calculated $P4mm$ structure has a tetragonality (c/a) of 1.04 and a volume of 60.2 \AA^3 , agreeing well with the experimental data and previous DFT calculations [30,31].

Electron doping is added into the structure with additional neutralizing background charges, instead of dopants like oxygen vacancies. In this case, however, the energy converges very slowly with respect to the size of the supercell. The problem is solved by adding a first order correction (image charge correction [32]) to the total energy. The phonon frequencies and the FCM's were calculated using the density functional perturbation theory [33] (DFPT) method as implemented in VASP and the phonopy [34] package. The nonanalytic contribution (NAC) [35] to the phonon and FCMs [36] was not considered. The Born effective charges (BEC's) for structures with free charges are not well defined, inhibiting the calculation of the NAC. The NAC only affects the longitudinal optical (LO) phonon frequencies, whereas the polar distortion is caused by the transverse optical (TO) phonon. We also checked the phonon results with NAC added against others' work [37], and the results agree well. The comparisons of BEC's and the Γ -point phonon frequencies for the $Pm\bar{3}m$ structure are in Table I and Table II, respectively. The Γ point FCMs were calculated in a $1 \times 1 \times 1 Pm\bar{3}m$ structure. A $2 \times 2 \times 2$ supercell of 40 atoms was used for the phonon band calculation.¹ The phonon frequencies were calculated with the structures fully relaxed. A Γ -centered $20 \times 20 \times 20$ Monkhorst-Pack grid was used to calculate the phonon density of states (PDOS). The crystal orbital hamilton population [38,39] (COHP) analyses were carried out with the LOBSTER [40] code. The crystal structures and the contour maps of the electron localization functions [41] (ELFs) were visualized using the VESTA package [42].

The ferroelectric polarization in a structure with free charges is not well defined. Therefore, the structural polar distortion is discussed instead of the ferroelectric polarization in the present work.

¹Although DFPT is capable of calculating the dynamic matrix at arbitrary wave vector without using supercells, only the Γ -point result is outputted in the VASP implementation. Phonopy makes use of the Γ point phonons of a larger supercell, maps them into a few wave vectors for the smaller cell, and then makes a Fourier interpolation to calculate the full phonon dispersion curve.

TABLE II. Γ -point phonon frequencies of PbTiO_3 in cubic structure with NAC added. The unit is THz. The results in Ref. [37] were calculated with LDA/DFPT.

	TO1	TO2	TO3	LO1	LO2	LO3
This work	3.84i	3.90	15.32	3.15	12.40	20.96
Ref. [37]	4.32i	3.63	14.90	3.12	12.30	20.18

III. RESULTS AND DISCUSSION

Here we show the enhancement of the polar distortion with electron doping in PbTiO_3 . The ferroelectric PbTiO_3 structure with $P4mm$ symmetry group is shown in Fig. 1, where the Pb and Ti cations displace along the c direction, and the O anions displace in the opposite direction. The change of the polar distortion in $P4mm$ PbTiO_3 structure with the concentration of the doped carriers (n_e) is shown in Fig. 2(a). As n_e increases, the tetragonality (c/a) of the lattice and the relative displacements of the Pb and Ti cations from the O anions increase. These phenomena show the enhancement of the polar distortion, in contrast to what happens in the $P4mm\text{BaTiO}_3$ [3–6], where the tetragonality and the cation-anion relative displacements both decrease to zero when the electron doping level is about 0.1 $e/u.c.$, as shown in Fig. 2(b). We also found that the lattice volumes increase with n_e in both PbTiO_3 and BaTiO_3 (Fig. 2). The polar distortion can be decomposed into three Γ -point normal modes [43–45] (Fig. 2), namely the Slater, Last, and Axe modes. The Slater mode [46] [Fig. 2(c)] involves the displacement of the Ti ion from the center of the oxygen octahedron, which is corresponding to the Ti-site instability. The Last mode [47] [Fig. 2(d)] involves the displacement of the A-site ions against the TiO_6 octahedron, which is corresponding to the A-site instability. The Axe mode [48] [Fig. 2(e)] involves the relative displacement of the O1 and O2 ions, which is corresponding to the distortion of the oxygen octahedron. It can be seen that in PbTiO_3 , both Slater mode and Last mode contribute to

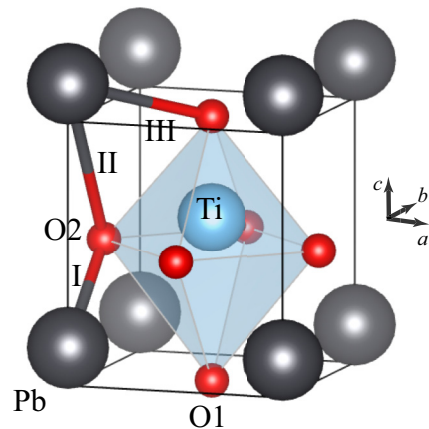


FIG. 1. The structure of $P4mm$ PbTiO_3 . The black, blue, and red spheres are the Pb, Ti, and O ions, respectively. O1 and O2 are the in-plane and apical oxygen ions, respectively. Due to the displacements of the ions in the c direction, there are two kinds of Pb-O2 bonds, the shorter one (type I) and the longer one (type II). The Pb-O1 bonds are labeled as type III.

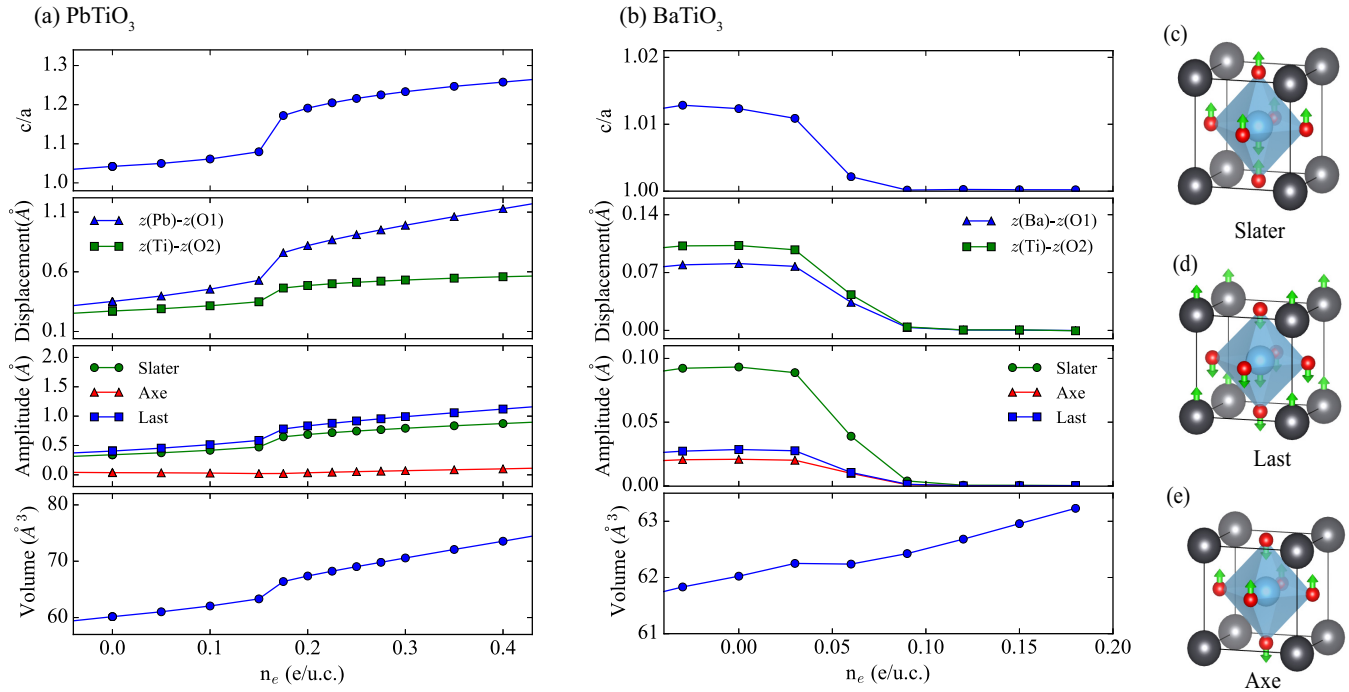


FIG. 2. The tetragonality (ratio of the out-of-plane lattice constant c and the in-plane lattice constant a), the relative displacements of Pb-O ($z(\text{Pb})-z(\text{O}1)$) and Ti-O ($z(\text{Ti})-z(\text{O}2)$), the amplitudes of the polar modes, and the volume as functions of doped electron density n_e in (a) PbTiO_3 and (b) BaTiO_3 , respectively. (c), (d), and (e) are the polar normal modes, namely the Slater, Last, and Axe modes.

the polar distortion. The amplitudes of them both increase as electrons are doped. For BaTiO_3 , Slater mode is predominant and decreases with electron doping. The difference implies that the Pb-site instability may drive the enhancement of the polar distortion in PbTiO_3 .

In our calculation, the doping level ranges from 0 to about 0.4 $e/\text{u.c.}$ Such a high doping level is hard or even impossible to be realized by adding dopants such as oxygen vacancies without changing the structural properties dramatically. Therefore, the results for high-doping levels presented here may not be applicable directly. However, it is still beneficial to see what happens in the hypothetical heavily doped structure in which the long-range Coulomb interaction should be mostly screened out.

In BaTiO_3 , the decreasing of the polar distortion with electron doping was believed to be because of the screening effect [5,6]. The doped electrons screen out the long-range Coulomb interaction. The screening length λ can be estimated with the Thomas-Fermi model $\lambda = \sqrt{\epsilon/e^2 D(E_F)}$, where ϵ is the dielectric permittivity, and $D(E_F)$ is the density of states (DOS) at the Fermi level. As the concentration of doped electrons increases, the DOS at the Fermi energy increases, and thus the screening length decreases. The values of ϵ and the values of $D(E_F)$ for PbTiO_3 are close to those for BaTiO_3 , respectively. $\epsilon(\text{PbTiO}_3)$ and $\epsilon(\text{BaTiO}_3)$ are $81\epsilon_0$ and $78\epsilon_0$ from the LDA/DFPT [49] calculation [50], respectively. When the concentration of electrons is 0.2 $e/\text{u.c.}$, the $D(E_F)$ are 0.7 and 1.1 states/(eV u.c.), and consequently the screening lengths are about 5 Å and 6 Å in PbTiO_3 and BaTiO_3 , respectively.) Therefore, the screening effects of the long-range Coulomb interaction are comparable in these two materials. The polar distortion is gradually destroyed by the screening effect in

BaTiO_3 . Then what is the intrinsic reason for the opposite trend of the polar distortion with doped electrons in PbTiO_3 to that in BaTiO_3 ?

Aside from the long-range Coulomb interaction, the covalence between Ti and O causes the Ti-site polar instability in both BaTiO_3 and PbTiO_3 . The difference is that the covalence between Pb-O also causes the Pb-site polar instability. Bersuker *et al.* interpreted both the Ti-site and Pb-site instabilities as the results of PJTE [23,24]. To see which site is responsible for the polar distortion and how the polar instabilities are affected by the electron doping, we consider the evolution of the phonon modes in the paraelectric $Pm\bar{3}m$ phase with the electron doping. The transition to a ferroelectric phase from a paraelectric phase is featured with imaginary phonon frequencies in the paraelectric phase. The phonon bands of $Pm\bar{3}m$ phase were calculated, as shown in Fig. 3. Without electron doping, the imaginary frequencies are at Γ , R , and M in the $Pm\bar{3}m$ phase, as shown in Fig. 3(a). With electrons doped, the imaginary frequency at the Γ point [Fig. 3(b)] corresponding to the ferroelectric distortion first decreases and then increases, as shown in Fig. 3(g), unlike that in BaTiO_3 [5], where the imaginary frequencies disappear as the concentration of electrons increases [Fig. 3(h)]. The atom projected phonon densities of states (PDOS) for $n_e = 0$ and $n_e = 0.2 e/\text{u.c.}$ are shown in Figs. 3(c) and 3(d), respectively. For both $n_e = 0$ and $n_e = 0.2 e/\text{u.c.}$, most of the PDOS in the imaginary frequency region is projected on the Pb sites, and a small portion is projected on the apical oxygen site O2, indicating that the soft phonons are from the Pb atoms and the O atoms in the side plane. The results are consistent with that the lone pair is from the Pb-O electron hybridization [51]. We also checked the phonon bands of the $P4mm$ phase with

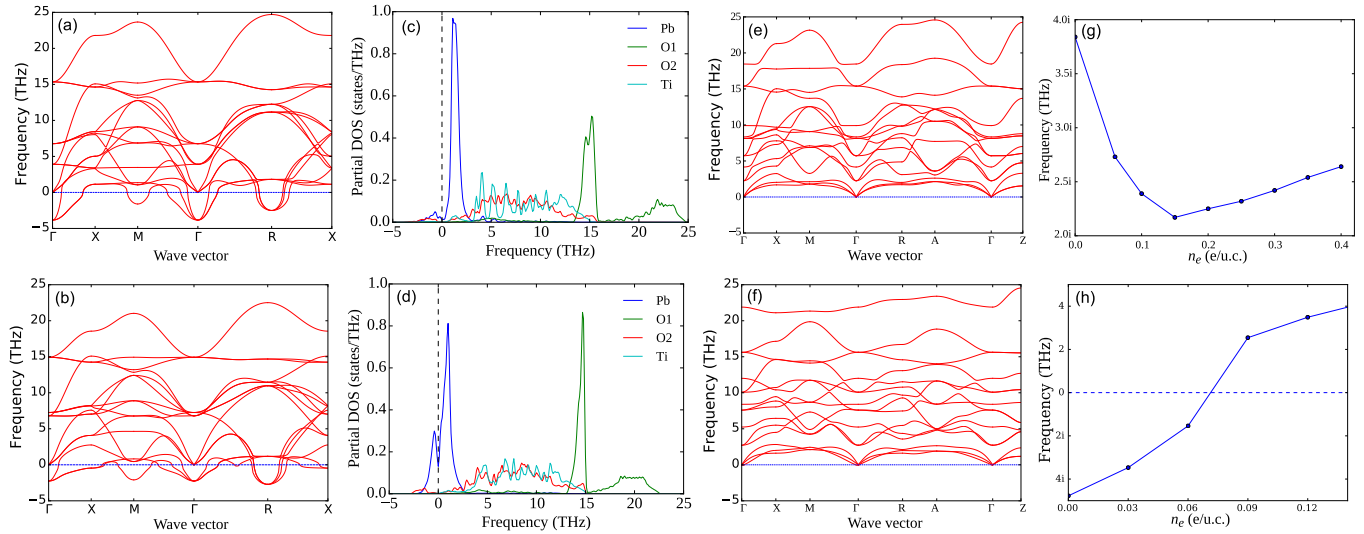


FIG. 3. The phonon band structures of the (a) $Pm\bar{3}m$ structure without doping, (b) $Pm\bar{3}m$ structure with electron doping ($n_e = 0.2 e/u.c.$), (e) $P4mm$ structure without doping, (f) $P4mm$ structure with electron doping ($n_e = 0.2 e/u.c.$). (c) and (d) are the atom projected partial phonon density of states projected on the [001] direction for the $Pm\bar{3}m$ structure without doping and with electron doping ($n_e = 0.2 e/u.c.$), respectively. In (a), (b), (c), and (d), the imaginary phonon frequencies are shown as negative numbers. The high symmetry q-vectors for $Pm\bar{3}m$ are Γ (0, 0, 0), X (0, 1/2, 0), M (1/2, 1/2, 0), R (1/2, 1/2, 1/2). The high symmetry q-vectors for $P4mm$ are Γ (0, 0, 0), X (0, 1/2, 0), M (1/2, 1/2, 0), R (0, 1/2, 1/2), A (1/2, 1/2, 1/2), Z (0, 0, 1/2). (g) and (h) are the lowest optic phonon frequencies at Γ as functions of the electron doping levels in $Pm\bar{3}m$ $PbTiO_3$ and $BaTiO_3$, respectively.

and without electron doping, and we found that there are no imaginary frequencies in the phonon bands in the $P4mm$ phase [Figs. 3(e) and 3(f)], indicating that the $P4mm$ phase is stable.

To further investigate the change of the lattice ferroelectric instabilities, we calculated the Γ point FCM's [52] (FCM's) of the $PbTiO_3$ and $BaTiO_3$ cubic structures with various concentration of doped electrons. The elements of the FCM $D_{ij}^{xy} = \partial^2 E / \partial u_i \partial u_j$ is the derivative of the energy with the displacements of two atoms u_i and u_j , where u_i is along the x direction and u_j is along the y direction. Due to the $Pm\bar{3}m$ symmetry, only the xx , yy , and zz components are nonzero. For the same i and j pair, the xx , yy , and zz components are equal to each other. So we only have to discuss the zz components here, i.e., the displacements are all along the z direction. Thus we omit the superscript of D_{ij}^{xy} . The changes of the FCMs are shown in Fig. 4.

For j equals to i , the element $\partial^2 E / \partial u_i^2$, which is the second derivative of the energy with the position of the atom, is known as self-force constants. A positive (negative) value of the self-force constant for an atom indicates an increasing (decreasing) of the energy by solely displacing that atom in the supercell with other atoms frozen. The self-force constants of $PbTiO_3$ and $BaTiO_3$ are shown in Figs. 4(a) and 4(b), respectively. In both $PbTiO_3$ and $BaTiO_3$, the self-force constants of Ti increase as n_e increases, which means that if the Ti atoms are displaced from their central symmetry positions, the energy costs would be higher, which reduces the Ti-site instability. In $PbTiO_3$, the self-force constant of Pb, which is the smallest among all self-force constants, decreases with n_e and eventually gets below zero, meaning that the tendency of Pb ions displacing from the central symmetry positions increases. In $BaTiO_3$, though the self-force constant of Ba ion also decreases with n_e , it is still much larger than zero, which stabilizes the Ba ion at the central symmetry position.

Then we look into the interatomic FC's (IFC's). The IFC's of $PbTiO_3$ and $BaTiO_3$ are shown in Figs. 4(d) and 4(e), respectively. A positive D_{ij} means that the energy would be lowered if the displacements of the two atoms labeled as i and j are along the different direction. It must be noted that an IFC is not corresponding to an individual bond but to the sum of all the interaction between two atoms, which may involve several bonds in a unit cell due to the periodic boundary condition. For example, if we consider only the nearest neighbor interaction, the Pb-O2 IFC is corresponding to the bonds of a Pb ion with the four nearest O2 ions, involving 2 type I Pb-O2 bonds and 2 type II Pb-O2 bonds. In $PbTiO_3$ and $BaTiO_3$, the polar distortions are featured with the antiparallel displacements of the cations (Pb, Ba, and Ti) and the anions (O), i.e., the positive values of cation-anion FC constants favor the polar distortion. In $BaTiO_3$, the antiparallel displacement of Ti and O1 is favored because of the Ti $3d$ -O1 $2p$ hybridization, therefore the IFC is positive. As n_e increases, the Ti-O1 interatomic FC decreases. In $PbTiO_3$, The Ti-O1 and Ti-O2 interatomic FC's also decrease. The decreasing of Ti-O IFC's and the increasing of the Ti self-force constants indicate that the Ti-site instability is reduced. The Pb-O and Ba-O IFC's increase with n_e in $PbTiO_3$ and $BaTiO_3$. But only the Pb-O2 IFC is above zero, which drives the Pb ions away from their central symmetry positions, whereas the Ba-O interaction cannot drive the polar distortion. The increasing of A-O FC's and the decreasing of the A-site self-force constants are the reasons for increasing of the A-site instability.

Both the Ti-site Pb-site instabilities can be viewed as results of PJTE's which will be referred to as Ti PJTE and Pb PJTE hereafter in this work, respectively. To see why their responses to the electron doping are different, we calculated the electronic structure of $PbTiO_3$.

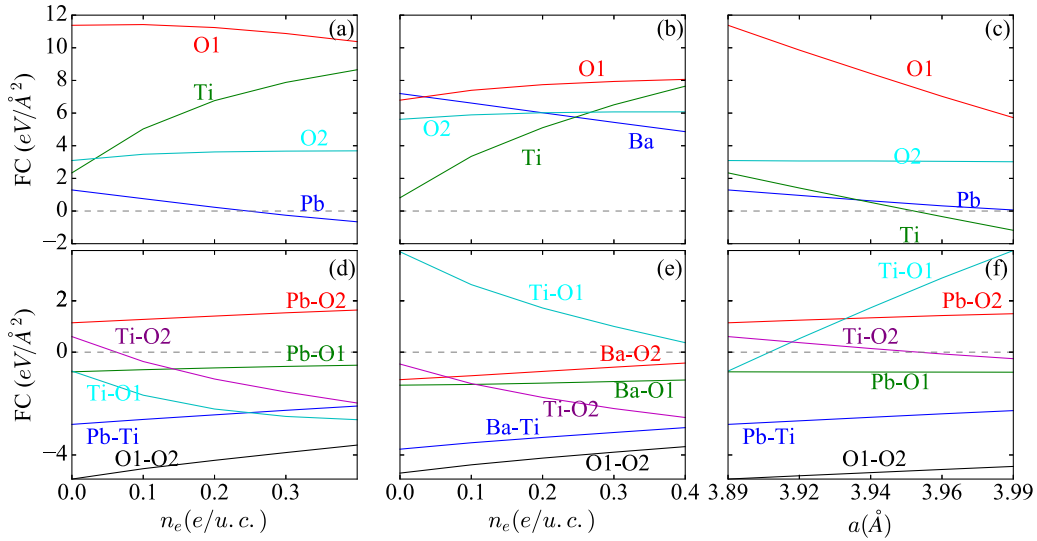


FIG. 4. Dependences of the FCM's on the concentration of doped electrons. (a) and (b) are the self-force constants on the different atoms in $Pm\bar{3}m$ $PbTiO_3$ and $BaTiO_3$, respectively. (d) and (e) are the IFC's between different pairs of atoms in $PbTiO_3$ and $BaTiO_3$, respectively. (c) and (f) are the self-force constants and the IFC's in the nondoped $Pm\bar{3}m$ $PbTiO_3$ structures, the lattice constants of which were fixed to these with electron doping. The lattice constants are corresponding to $n_{el} = 0.0-0.4$ e/u.c.

PJTE is through a mix of the ground state and the low excited states by vibronic coupling. Detailed descriptions of PJTE are in the works of Bersuker *et al.* [23–25]. In a high-symmetry $Pm\bar{3}m$ reference system, the energy E can be written as a function of a normal displacement q , where $\partial E/\partial q = 0$. If the curvature K of the energy E , $K = (\partial^2 E/\partial q^2)_0$, is negative, the energy is at a local maximum, indicating that the system is unstable. K can be written as the sum of a positive frozen part K_0 and a negative vibronic part K_v . Using the second order perturbation theory, K_v can be written as

$$K_v = -2 \sum_n \frac{|\langle \psi_0 | (\partial H/\partial q)_0 | \psi_n \rangle|^2}{E_n - E_0}, \quad (1)$$

in which ψ_0 is the ground state, ψ_n is an excited state, and E_n and E_0 are the energies of the excited state and the ground state, respectively. It can be noticed that $K_v < 0$ if the mix of the ground state and the excited state under the displacement q is allowed by symmetry. Thus K_v contributes to the instability. If the parity of the product of the ground state and the excited state is odd, the net overlap of them would be zero in the highest symmetry. However, with a polar vibration, the hybridization becomes nonzero, causing an energy gain. Therefore, the BJTE can be interpreted as added covalence in terms of bonding [26].

The instability of Ti atoms is due to the PJTE [23–25]. In the TiO_6 octahedron with Ti d^0 electronic configuration, the highest occupied states and the lowest unoccupied states are mostly O $2p$ and Ti $3d$, respectively. The product of them is odd so their contribution to K_v is nonzero, which can cause the PJTE. The “ d^0 ness” plays an essential role in this kind of PJTE. Electron doping pushes the Fermi energy into the bottom of the conduction band, which is mostly Ti $3d$ [Fig. 5(a)]. The Ti $3d$ -Ti $3d$ product is even, therefore it makes no contribution to the lattice instability. Thus, the Ti PJTE is suppressed as the electron doping increases.

The lone-pair mechanism of the ferroelectric materials with cations of s^2p^0 electronic configuration is another kind of PJTE [53,54]. Regarding the Pb-O bonds, the electronic

states near the Fermi energy are the Pb $6s$ and $6p$ states, and the O $2p$ states. The occupied Pb $6s$ orbitals and the O $2p$ orbitals form bonding states with energies of about -10 eV [region (i) in Fig. 5(b)], and the antibonding states just below the Fermi energy [region (iii) in Fig. 5(b)]. These occupied (Pb $6s$)-(O $2p$) antibonding states can be seen as the ground states in equation (1), whereas the Pb $6p$ states are the unoccupied excited states. The overlap of them has both positive and negative parts, which cancel out in the central symmetric cubic structure. The mixing between the ground and excited states becomes nonzero if Pb moves away from the central-symmetric position, which lowers the total energy and thus drives the polar distortion. The hybridization between the (Pb $6s$ -O $2p$) bonding states with Pb $6p$ states results in bonding and antibonding states, corresponding to the region (ii) and region (iv), respectively. Therefore, the Pb PJTE effect can also be interpreted as added covalence [26] in the terms of bonding, which is believed to be the driving force for the Pb-site instability [19,52]. The displacement of Pb reduces the type I Pb-O bond, leading to a strong covalency between Pb and O2 ions. The hybridization also causes the asymmetric ELF lobes near the Pb sites as shown in Figs. 5(c) and 5(d), which is a characteristic of the lone-pair mechanism [51,55].

As can be seen from Figs. 5(a) and 5(b), the unoccupied Pb $6p$ states, which are the excited states involved in the Pb PJTE, are above the Fermi energy when the electrons are doped. Therefore, the Pb PJTE will not be strongly affected by the electron doping. As a result, the change of the Pb self-force constant with electron doping is much smaller than that of Ti; the change of the Pb-O interatomic force constants are also much smaller than those of Ti-O, as shown in Fig. 4. There's no significant reduction in the asymmetric lobe of the ELFs in the doped structure [Fig. 5(d)] comparing with that in the nondoped structure [Fig. 5(c)].

The increasing of the Pb site instability is likely to be the result of the elongation of the Pb-O distance with electron doping. The forces between the doped electrons on the Ti $3d$

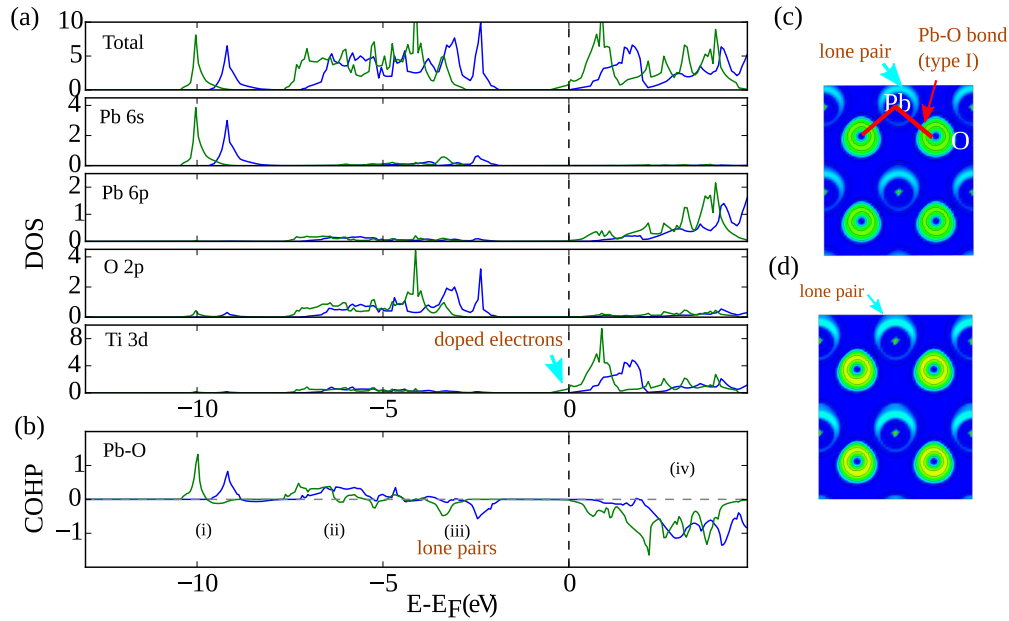


FIG. 5. (a) The density of states in PbTiO_3 . (b) The COHP of the Pb-O bond. In (a) and (b), the blue lines and the green lines represent the results in the nondoped and doped PbTiO_3 structures, respectively. The results for nondoped structure are shifted so that the Fermi energy is at the conduction band minimum. The concentration of the doped electrons is $n_e = 0.2 e/u.c.$ (c) and (d) are the contour maps of the ELFs in the $a - c$ PbO plane of the doped and nondoped structures, respectively.

bands and the negatively charged O anions are repulsive, which increases the Ti-O bond lengths so the Pb-O distances are also increased. Thus the overlap of the Pb and O orbitals decreases, which will lead to the decreasing of both $|K_0|$ and $|K_v|$. If $|K_0|$ decreases more quickly than $|K_v|$, the instability will increase, which is the case in Ti PJTE in titanates $RTiO_3$ ($R = \text{Ba}, \text{Sr}, \text{Ca}$) [56]. In terms of bonding, the PJTE can be interpreted as added covalent interaction. In perovskites, a tolerance factor t smaller (larger) than 1 implies an underbonded A (B) site ion [57]. The PJTE is effective when the added covalent interaction reduces the total energy, which tends to happen for an underbonded ion. The increasing of B-site ion size decreases t , thus the A-site ion becomes more underbonded, which tends to enhance the PJTE. To test whether the enhancement of A-site instability is due to the increased Pb-O distance, we calculated the IFC's of PbTiO_3 without electron doping, and the lattice constants of the structures were fixed to those with electron doping. The results are in Figs. 4(c) and 4(f). Indeed, the self-force constants of Pb, the IFC's of Pb-O1 and Pb-O2 in the nondoped structures, are almost identical to those with electron doping, which confirmed that the enhanced Pb-site instability is due to the increased Pb-O distance. The self-force constant of Ti decreases and the Ti-O1 IFC increases in the nondoped structure, just opposite to the trends in the doped structures. This further shows that the increased occupation of the Ti 3d bands is the reason for the decreased Ti-site instability in PbTiO_3 .

We also noted that the change of the polar distortion with electron doping is very similar to that with the negative hydrostatic pressure in PbTiO_3 . In both cases, the Pb-O bonds are stretched. We calculated the changes of the polar distortion of PbTiO_3 with negative hydrostatic pressure. The polar distortion increases with negative hydrostatic pressure in PbTiO_3 , which agrees with previous studies [58–60]. The

changes of the distortion with electron doping were plotted as functions of lattice volume and then compared to those with hydrostatic pressure, as shown in Fig. 6. The changes of c/a and cation-anion displacements with the same lattice volume are close in the two situations, indicating that the enhancement of the polar distortion might be from the same origin. It can also be seen that there is an anomalous enhancement of tetragonality and lattice volume as n_e increases to about $0.3 e/u.c.$ (Fig. 2), which was also found in PbTiO_3 with negative pressure [58]. The polar distortions in the electron-doped structure are smaller than those in the nondoped structures with the same volume, which may be the result of the screening effect.

It is interesting to note that the changes of polar distortion with negative hydrostatic pressure and those with electron doping are opposite in BaTiO_3 , where the polar distortion also increases with the negative hydrostatic pressure [58,59], but decreases with the electron doping, though the volumes both increase in these two situations [5,58,59]. The Ti-O bonds are stretched in the structure with negative hydrostatic pressure, therefore Ti becomes more underbonded, which requires a larger polar distortion. Whereas in the electron-doped structure, the Ti-O short-range repulsion is enhanced due to the electrons on the Ti 3d bands and the suppression of Ti PJTE, leading to the reduced Ti-site instability. In both cases, the Ba-O bonds are stretched, leading to the enhanced Ba-O instability, which is however not enough to result in a polar distortion in electron-doped BaTiO_3 . Consequently, the polar distortion in BaTiO_3 decreases with electron doping. It can be seen that the changes of polar distortion in BaTiO_3 and PbTiO_3 can be uniformly viewed as the results of the decreased of A-site instability and increased B-site instability.

We examined the Pb-O bonds to see how the stretching of the Pb-O bonds affects the polar distortion. The lengths of the

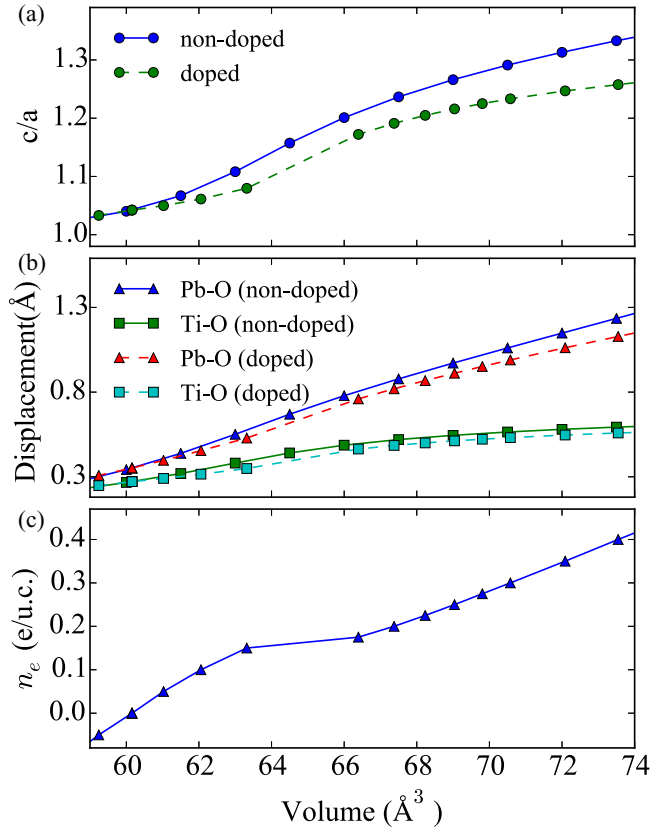


FIG. 6. (a) The ratio c/a as the function of lattice volume. (b) The relative displacements of Pb-O ($z(\text{Pb}) - z(\text{O1})$) and Ti-O ($z(\text{Ti}) - z(\text{O2})$) as functions of lattice volume. (c) The concentration of the doped electrons corresponding to the volume. The results for the nondoped structures were calculated by imposing negative hydrostatic pressure.

Pb-O bonds are plotted in Fig. 7. As the doped electrons enlarge the sizes of Ti ions and the lengths of Ti-O bonds, the Pb-O chain consisting of alternating type I and type II bonds are stretched. The changes of the type I bond lengths are relatively small, while those of the type II bond lengths are much larger.

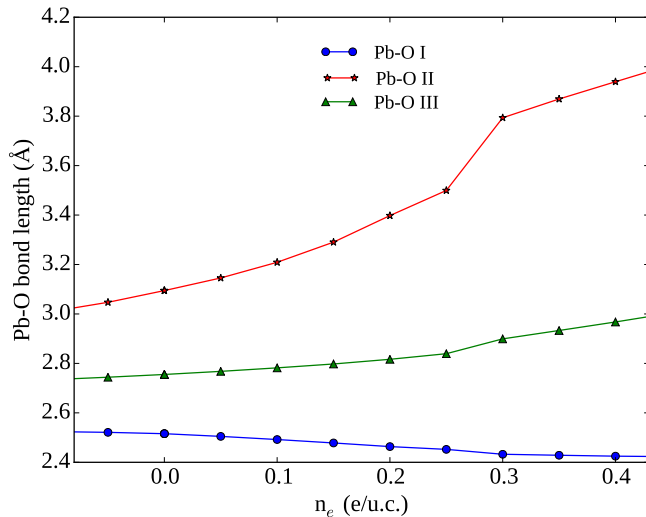


FIG. 7. The change of lengths of the Pb-O bonds with the concentration of doped electrons.

The reason is that the Pb-O electron hybridization stabilizes the short Pb-O type I bonds, and the enhanced Pb PJTE causes a larger displacement of Pb towards the side of type I bonds.

There are some similarities between the electron-doped PbTiO_3 and the NCSM LiOsO_3 . Firstly, the A-site instability drives the polar distortion. Secondly, in both structures, the polar instabilities are due to the short-range interactions, which is the PJTE (or equivalently, the covalent interaction) for PbTiO_3 , and short-range Coulomb interaction for LiOsO_3 . Thirdly, the Fermi energy is in the B-site bands and outside the energy range of the electronic states related to the A-O interaction. In LiOsO_3 , it was found that the ferroelectricity is due to the Li-O displacement, whereas the Fermi level lies in the Os bands [9–12]. These similarities infer that the polar distortion caused by short-range interactions and the metallicity can coexist.

The mechanism of the persistent or even the enhancement of the polar distortion in PbTiO_3 with electron doping presented in this paper should be transferable to other lone-pair driven ferroelectric materials, like in PbVO_3 [61], BiFeO_3 [62,63], SnTiO_3 [51], and BiMnO_3 [55]. In these materials, the electronic states corresponding to the lone-pair mechanism are away from the Fermi energy if electrons are doped, whereas the bottom of conduction bands in these materials are often the B-site states. Thus the doping of electrons can be seen as a selective enlargement of the B-site ion radius, which stretches the A-O bonds. Therefore, enhancement of polar distortion in these materials similar to that in PbTiO_3 is likely to emerge. These results also imply that the lone-pair stereoactive ions can be used as the A-site ions in perovskites to form NCSMs. By selecting a B-site element (or elements) with suitable ionic radius and itinerant electrons, lone-pair driven non-central-symmetric metal may be designed.

IV. CONCLUSION

In this paper, we investigated the effect of electron doping on the lone-pair driven polar distortion by carrying out density functional theory studies on PbTiO_3 . We found that the polar distortion is enhanced with electron doping in PbTiO_3 even when the long-range Coulomb interaction is screened out by the doped electrons. The analysis on the phonons and electronic states shows the mechanism for the persistence of the polar distortion: The lone-pair mechanism, which is the driving force of the polar distortion, is not strongly affected by the electron doping because the energy range of the related electron states is far enough from the Fermi energy. We also found that the enhancement of the polar distortion in PbTiO_3 is due to the increasing of the Ti ion radius, which caused the increasing of the Pb-O distance. These results show that the lone-pair driven polar distortion and the metallicity can coexist, and it is highly expected that the lone-pair stereoactive ions can be used in designing NCSMs.

ACKNOWLEDGMENTS

The work was supported by the National Basic Research Program of China (Grants No. 2014CB921001 and No. 2012CB921403), the National Natural Science Foundation of China (Grant No. 11134012), and the Strategic Priority Research Program (B) of the Chinese Academy of Sciences (Grant No. XDB07030200).

- [1] W. Cochran, *Adv. Phys.* **9**, 387 (1960).
- [2] P. Ghosez, X. Gonze, and J.-P. Michenaud, *Europhys. Lett.* **33**, 713 (1996).
- [3] L. Liu, H. Guo, H. Lu, S. Dai, B. Cheng, and Z. Chen, *J. Appl. Phys.* **97**, 054102 (2005).
- [4] K. Page, T. Kolodiazny, T. Proffen, A. K. Cheetham, and R. Seshadri, *Phys. Rev. Lett.* **101**, 205502 (2008).
- [5] Y. Wang, X. Liu, J. D. Burton, S. S. Jaswal, and E. Y. Tsymlal, *Phys. Rev. Lett.* **109**, 247601 (2012).
- [6] Y. Iwazaki, T. Suzuki, Y. Mizuno, and S. Tsuneyuki, *Phys. Rev. B* **86**, 214103 (2012).
- [7] P. W. Anderson and E. I. Blount, *Phys. Rev. Lett.* **14**, 217 (1965).
- [8] Y. Shi, Y. Guo, X. Wang, A. J. Princep, D. Khalyavin, P. Manuel, Y. Michiue, A. Sato, K. Tsuda, S. Yu *et al.*, *Nat. Mater.* **12**, 1024 (2013).
- [9] H. Sim and B. G. Kim, *Phys. Rev. B* **89**, 201107 (2014).
- [10] H. J. Xiang, *Phys. Rev. B* **90**, 094108 (2014).
- [11] G. Giovannetti and M. Capone, *Phys. Rev. B* **90**, 195113 (2014).
- [12] H. M. Liu, Y. P. Du, Y. L. Xie, J.-M. Liu, C.-G. Duan, and X. Wan, *Phys. Rev. B* **91**, 064104 (2015).
- [13] D. Puggioni and J. M. Rondinelli, *Nat. Commun.* **5**, 3432 (2014).
- [14] N. A. Benedek and T. Birol, *J. Mater. Chem. C* **4**, 4000 (2016).
- [15] V. P. Mineev and Y. Yoshioka, *Phys. Rev. B* **81**, 094525 (2010).
- [16] V. M. Edelstein, *Phys. Rev. B* **83**, 113109 (2011).
- [17] V. M. Edelstein, *Phys. Rev. Lett.* **75**, 2004 (1995).
- [18] V. M. Edelstein, *J. Phys. Condens. Matter* **8**, 339 (1996).
- [19] R. E. Cohen, *Nature (London)* **358**, 136 (1992).
- [20] R. E. Cohen and H. Krakauer, *Ferroelectrics* **136**, 65 (1992).
- [21] Y. Kuroiwa, S. Aoyagi, A. Sawada, J. Harada, E. Nishibori, M. Takata, and M. Sakata, *Phys. Rev. Lett.* **87**, 217601 (2001).
- [22] H. Tanaka, Y. Kuroiwa, and M. Takata, *Phys. Rev. B* **74**, 172105 (2006).
- [23] I. Bersuker, *Phys. Lett.* **20**, 589 (1966).
- [24] I. B. Bersuker and B. G. Vekhter, *Ferroelectrics* **19**, 137 (1978).
- [25] I. Bersuker, *The Jahn-Teller Effect* (Cambridge University Press, Cambridge, 2006).
- [26] I. B. Bersuker, *Chem. Rev.* **113**, 1351 (2013).
- [27] G. Kresse and D. Joubert, *Phys. Rev. B* **59**, 1758 (1999).
- [28] G. Kresse and J. Furthmüller, *Phys. Rev. B* **54**, 11169 (1996).
- [29] J. P. Perdew and A. Zunger, *Phys. Rev. B* **23**, 5048 (1981).
- [30] G. Shirane, R. Pepinsky, and B. C. Frazer, *Acta Crystallogr.* **9**, 131 (1956).
- [31] G. Sághi-Szabó, R. E. Cohen, and H. Krakauer, *Phys. Rev. Lett.* **80**, 4321 (1998).
- [32] S. Lany and A. Zunger, *Phys. Rev. B* **78**, 235104 (2008).
- [33] S. Baroni, S. de Gironcoli, A. Dal Corso, and P. Giannozzi, *Rev. Mod. Phys.* **73**, 515 (2001).
- [34] A. Togo and I. Tanaka, *Scr. Mater.* **108**, 1 (2015).
- [35] X. Gonze and C. Lee, *Phys. Rev. B* **55**, 10355 (1997).
- [36] R. M. Pick, M. H. Cohen, and R. M. Martin, *Phys. Rev. B* **1**, 910 (1970).
- [37] W. Zhong, R. D. King-Smith, and D. Vanderbilt, *Phys. Rev. Lett.* **72**, 3618 (1994).
- [38] R. Dronskowski and P. E. Bloechl, *J. Phys. Chem.* **97**, 8617 (1993).
- [39] V. L. Deringer, A. L. Tchougréeff, and R. Dronskowski, *J. Phys. Chem. A* **115**, 5461 (2011).
- [40] S. Maintz, V. L. Deringer, A. L. Tchougréeff, and R. Dronskowski, *J. Comput. Chem.* **34**, 2557 (2013).
- [41] J. Íñiguez, D. Vanderbilt, and L. Bellaiche, *Phys. Rev. B* **67**, 224107 (2003).
- [42] K. Momma and F. Izumi, *J. Appl. Crystallogr.* **41**, 653 (2008).
- [43] J. H. Lee and K. M. Rabe, *Phys. Rev. B* **84**, 104440 (2011).
- [44] J. Hong, A. Stroppa, J. Íñiguez, S. Picozzi, and D. Vanderbilt, *Phys. Rev. B* **85**, 054417 (2012).
- [45] H. Wang, J. Wen, D. J. Miller, Q. Zhou, M. Chen, H. N. Lee, K. M. Rabe, and X. Wu, *Phys. Rev. X* **6**, 011027 (2016).
- [46] J. C. Slater, *Phys. Rev.* **78**, 748 (1950).
- [47] J. T. Last, *Phys. Rev.* **105**, 1740 (1957).
- [48] J. D. Axe, *Phys. Rev.* **157**, 429 (1967).
- [49] X. Wu, D. Vanderbilt, and D. R. Hamann, *Phys. Rev. B* **72**, 035105 (2005).
- [50] H. Moriwake, C. A. J. Fisher, A. Kuwabara, and T. Hashimoto, *Jpn. J. Appl. Phys.* **50**, 09NE02 (2011).
- [51] K. C. Pitike, W. D. Parker, L. Louis, and S. M. Nakhmanson, *Phys. Rev. B* **91**, 035112 (2015).
- [52] P. Ghosez, E. Cockayne, U. V. Waghmare, and K. M. Rabe, *Phys. Rev. B* **60**, 836 (1999).
- [53] I. B. Bersuker, *Ferroelectrics* **164**, 75 (1995).
- [54] A. Walsh, D. J. Payne, R. G. Egdell, and G. W. Watson, *Chem. Soc. Rev.* **40**, 4455 (2011).
- [55] R. Seshadri and N. A. Hill, *Chem. Mater.* **13**, 2892 (2001).
- [56] I. B. Bersuker, N. N. Gorinchoi, and T. A. Fedorco, *Ferroelectrics* **153**, 1 (1994).
- [57] M. Ghita, M. Fornari, D. J. Singh, and S. V. Halilov, *Phys. Rev. B* **72**, 054114 (2005).
- [58] S. Tinte, K. M. Rabe, and D. Vanderbilt, *Phys. Rev. B* **68**, 144105 (2003).
- [59] H. Moriwake, Y. Koyama, K. Matsunaga, T. Hirayama, and I. Tanaka, *J. Phys. Condens. Matter* **20**, 345207 (2008).
- [60] J. Wang, B. Wylie-van Eerd, T. Sluka, C. Sandu, M. Cantoni, X.-K. Wei, A. Kvasov, L. J. McGilly, P. Gemeiner, B. Dkhil *et al.*, *Nat. Mater.* **14**, 985 (2015).
- [61] D. J. Singh, *Phys. Rev. B* **73**, 094102 (2006).
- [62] P. Ravindran, R. Vidya, A. Kjekshus, H. Fjellvåg, and O. Eriksson, *Phys. Rev. B* **74**, 224412 (2006).
- [63] X. He, K. J. Jin, H. Z. Guo, and C. Ge, *Phys. Rev. B* **93**, 174110 (2016).